

**Performance improvement by alumina coatings on $Y_3Al_5O_{12}$
 Ce^{3+} phosphor powder deposited using atomic layer deposition in a fluidized bed reactor**

Zhou, Zhi; Zhou, Nan; Lu, Xiangyang; Kate, Melvin Ten; Valdesueiro Gonzalez, D.; van Ommen, J.R.; Hintzen, H. T.

DOI

[10.1039/c6ra12983h](https://doi.org/10.1039/c6ra12983h)

Publication date

2016

Document Version

Accepted author manuscript

Published in

RSC Advances

Citation (APA)

Zhou, Z., Zhou, N., Lu, X., Kate, M. T., Valdesueiro Gonzalez, D., van Ommen, J. R., & Hintzen, H. T. (2016). Performance improvement by alumina coatings on $Y_3Al_5O_{12}$: Ce^{3+} phosphor powder deposited using atomic layer deposition in a fluidized bed reactor. *RSC Advances*, 6(80), 76454-76462. <https://doi.org/10.1039/c6ra12983h>

Important note

To cite this publication, please use the final published version (if applicable). Please check the document version above.

Copyright

Other than for strictly personal use, it is not permitted to download, forward or distribute the text or part of it, without the consent of the author(s) and/or copyright holder(s), unless the work is under an open content license such as Creative Commons.

Takedown policy

Please contact us and provide details if you believe this document breaches copyrights. We will remove access to the work immediately and investigate your claim.

1 **Performance improvement by alumina coatings on**
2 **$Y_3Al_5O_{12}:Ce^{3+}$ phosphor powder deposited using Atomic**
3 **Layer Deposition in a fluidized bed reactor**

4
5 Zhi Zhou¹, Nan Zhou*¹, Xiangyang Lu*², Melvin ten Kate³, David Valdesueiro⁴, J. Ruud van
6 Ommen³, H.T. (Bert) Hintzen⁴

7
8 1 Science College of Hunan Agricultural University, Changsha 410128, China

9 2 College of Bioscience and Biotechnology, Hunan Agricultural University, Changsha 410128,
10 China

11 3 Department of Chemical Engineering, Delft University of Technology, Van der Maasweg 9,
12 2629 HZ Delft, The Netherlands

13 4 Group Luminescent Materials, Section Fundamental Aspects of Materials and Energy, Faculty of
14 Applied Sciences, Delft University of Technology, The Netherlands

15

16 Corresponding authors: Dr. Nan Zhou, Email: zhounan@hunau.edu.cn;

17 Prof. Xiangyang Lu, Email: xiangyangcn@163.com.

18

19

20 **Abstract:**

21 To improve the thermal stability, Al_2O_3 has been successfully coated on a $Y_3Al_5O_{12}:$
22 Ce^{3+} (YAG:Ce) phosphor powder host by using the Atomic Layer Deposition (ALD)
23 approach in a fluidized bed reactor. Transmission Electron Microscopy (TEM) and
24 Energy Dispersive X-ray spectroscopy (EDX) analysis indicate that coating an Al_2O_3
25 thin layer by ALD is highly feasible. The luminescence properties (such as excitation
26 and emission as well as quantum efficiency and UV-absorption of the coated YAG:Ce
27 phosphor) were systematically analysed, with the further examination of the thermal
28 resistance characteristics. The Al_2O_3 thin layer coating with precisely controlled
29 thickness by ALD can obviously improve the luminescence intensity and greatly
30 enhances the thermal stability of the YAG:Ce phosphor. It is suggested that the
31 alumina coating with tailoring thickness seems not only to act like a barrier to
32 decrease the thermal quenching, but also as a great help to promote the light
33 absorption and transfer.

34

35 Key words: Atomic Layer Deposition (ALD), fluidized bed reactor, YAG:Ce,
36 phosphor, powder coating, thermal stability.

37

38

39

40

41 1 Introduction

42 Inorganic luminescent materials, or phosphors, are commonly utilized for many
43 applications such as monitors, fluorescent lamps, plasma displays, X-ray amplifier
44 screens, Light Emitting Diodes (LEDs), and electroluminescent displays due to their
45 cathodo-, photo-, X-ray- or electro-luminescence properties¹⁻³. However, the
46 instability of the phosphors against temperature, oxygen, water, acids, etc. remains a
47 problem, which significantly hinders their processing, storage as well as the
48 applications².

49 Coating a phosphor with a protective layer has been proved to be an efficient
50 approach to protect a phosphor from environmental attack⁴⁻¹². Thus, several
51 techniques have been explored to deposit coating layers on phosphor. Including 1)
52 solid-state techniques such as rolling, milling, grinding of mixtures of phosphor
53 powders with the precursor, followed by drying or a heat treatment if necessary; 2)
54 liquid-phase techniques such as sol-gel⁴⁻⁶, emulsion⁷, hetero-coagulation⁸, and
55 precipitation⁹; and 3) gas-phase techniques such as Chemical Vapor Deposition
56 (CVD)¹⁰, Pulsed Laser Deposition (PLD)¹¹, and Atomic Layer Deposition (ALD)^{12, 13}.
57 However, most of the conventional coating methods suffer from inhomogeneous
58 and/or ununiformed coating layer deposition, which will have a negative effect on the
59 optical properties⁶. Therefore, a closed thin film coating method is needed in order to
60 protect phosphor particles while maintaining (or even improving) the optical
61 properties.

62 ALD is well known for depositing thin films on a flat surface, but with the
63 combination of a fluidized bed reactor, it can also be used for coating micro and
64 nano-sized powders¹⁴. In such a fluidized bed reactor the particles are suspended in an
65 upward gas flow so that good contact between gas and particles is ensured. Besides
66 thin but nevertheless closed coating, another main advantage of ALD is that the
67 thickness of a coated layer can be precisely designed by strictly controlling the
68 number of ALD cycles. Thus, ALD can supply a uniform coating even on high surface
69 area materials allowing a variation of thickness at an atomic resolution, all of which
70 benefits ALD as a suitable method for homogeneous ultrathin layer deposition¹⁵. Li et
71 al.¹⁶ successfully deposited a 15 nm TiO₂ thin film on Cu₂O-based photocathodes
72 through ALD method after ALD coating of an appropriate 20 nm buffer layer of
73 Ga₂O₃ on Cu₂O microcrystals. The high thermal resistance of Ga₂O₃ allowed for the
74 double coating at relatively high temperatures, resulting in a better photo-voltage of
75 the whole active cathode. A thin 1.2 nm TiO₂ coating was performed by ALD on
76 cobalt particles to prevent both leaching and sintering during aqueous-phase reactions.
77 The TiO₂/Co/TiO₂ composite showed a high catalysis activity for aqueous-phase
78 hydrogenation reactions with excellent stability¹⁷. All above demonstrate that ALD
79 techniques can produce continuous, pinhole-free oxide films with
80 Angstrom-level-controllable thickness. Especially within a fluidized bed reactor, ALD
81 shows high potential for depositing a protective thin layer coating on a phosphor
82 particle without hurting the optical properties.

83 Many kinds of the oxides, such as Al₂O₃¹⁸⁻²⁰, SiO₂^{21, 22}, TiO₂^{23, 24}, ZnO^{25, 26}, and
84 ZrO₂²⁷ have been used as coating material in ALD processes. Among them, Al₂O₃ is

85 considered to be a promising coating agent to enhance the resistance of the coated
86 materials. For example, the capacity fading of LiMn_2O_4 spinel as a battery material
87 can be significantly reduced due to Al_2O_3 coating and consistent discharge curves
88 were found even after 50 charging/discharging cycles at an elevated temperature of 55°C
89 ²⁸. Ultrathin compact Al_2O_3 layers deposited by ALD were also utilized to improve
90 the ambient stability of quantum dot films²⁹ and organic-inorganic perovskite solar
91 cells²⁰. The results demonstrate that the stability of the solar cell against humidity was
92 greatly enhanced without an obvious reduction in efficiency. Besides, Al_2O_3
93 demonstrates a unique affinity to a large variety of substrate¹⁴, together with its low
94 deposition temperature, led to the judgments that depositing Al_2O_3 as a coating via
95 ALD in a fluidized bed reactor is a promising way to increase resistance against
96 outside attacks resisted for phosphor materials like $\text{Y}_3\text{Al}_5\text{O}_{12}:\text{Ce}^{3+}$.

97 $\text{Y}_3\text{Al}_5\text{O}_{12}:\text{Ce}^{3+}$ (the trivalent cerium activated Yttrium Aluminate phosphor with
98 Garnet structure, referred to as YAG:Ce), is a well-known luminescent material which
99 has been broadly applied in the fields of flying spot scanner tubes in the past and
100 white LED (WLED) devices nowadays. However, like most of the luminescence
101 phosphors, YAG:Ce also suffers from the thermal instability, especially when used in
102 practical WLED devices³. In this work, YAG:Ce phosphor powder is employed as
103 model material to study the improvement of the thermal stability by Al_2O_3 coating
104 through ALD process performed in a fluidized bed reactor under atmospheric pressure.
105 The impact of ALD cycle numbers on the thickness of the Al_2O_3 layer is investigated,
106 as well as the thermal and optical performance of YAG:Ce phosphor. It will be shown
107 that the ALD method with a fluidized bed reactor using alumina as oxide coating
108 materials could be a feasible way for the ultrathin film coating of YAG:Ce phosphors
109 and apply a protective barrier for improving thermal resistance while maintaining the
110 optical properties.

112 2 Experimental

113 2.1 Starting materials

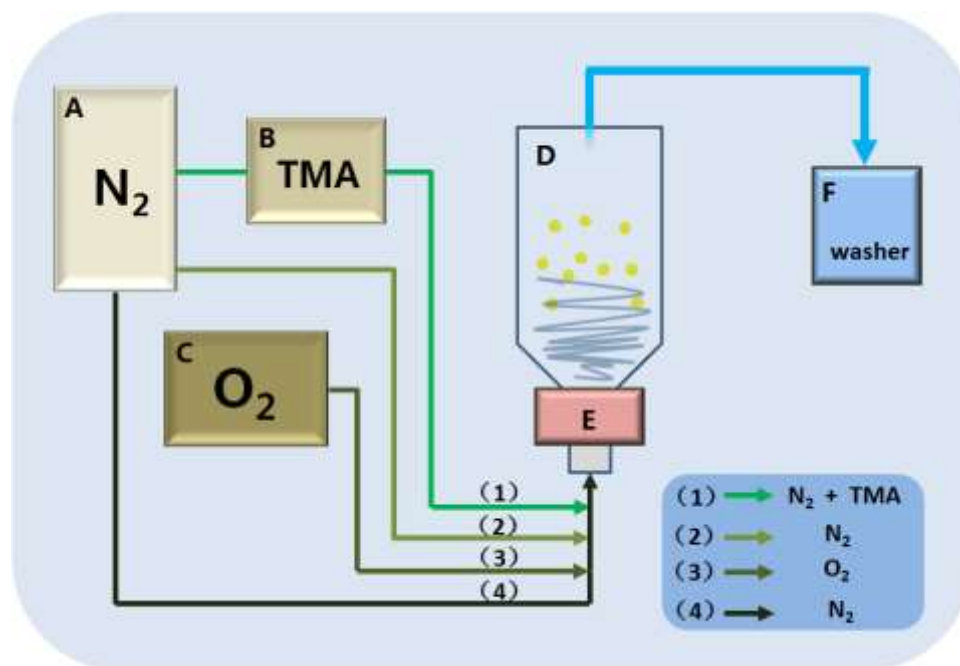
114 The YAG:Ce phosphor particles were obtained from Steady (Hunan Steady New
115 Materials Company, China), which have a regular spherical morphology with highly
116 concentrated particle size distribution between 6-15 micrometers.
117 Tri-Methyl-Aluminium (TMA, semiconductor grade) was supplied by Akzo-Nobel
118 HPMO in a 400mL VER-400 bubbler. The gas washers were filled with Kaydol oil,
119 supplied by Sonneborn (Haarlem).

121 2.2 Sample preparation by ALD coating process in a fluidized bed reactor

122 A schematic illustration of the ALD set-up with a fluidized bed reactor for the
123 alumina coating on YAG:Ce particle is shown in Fig. 1. From left to right, Part A is a
124 nitrogen gas tank supplying a nitrogen flow. Part B is a bubbler filled with liquid
125 TMA, through which nitrogen is bubbled to obtain a nitrogen flow with TMA vapor.
126 Part C is a gas bottle filled with an N_2/O_2 mixture (80%/20%). Part D is the Fluidized
127 Bed Reactor (FBR), the main part of which is a glass column with 26 mm in internal
128 diameter and 500 mm in length. Only less than one third volume of the column can be

129 filled with certain amount (100-120g) of phosphor particles, in order to guarantee
130 enough space for the particles during fluidizing. The FBR is placed on a vibration
131 table driven by two vibro-motors (Part E), which can produce a low amplitude
132 vibration at a set frequency of 45 Hz to assist fluidization. The coating experiments
133 were carried out at room temperature of about 25°C. And Part F represents the gas
134 washers to neutralize TMA that might be released from the reactor.

135 Generally, one ALD cycle can be divided into four process steps: (1) TMA
136 exposure, (2) purge with nitrogen gas, (3) oxygen exposure and (4) purge with
137 nitrogen gas again. To begin with the whole ALD set needs to be purged with nitrogen
138 for about 20 min before starting the first ALD cycle. For the first step of TMA
139 exposure, nitrogen was purged through the reactant bubbler (Part B) filled with TMA
140 and making a gas stream for carrying the reactant into the FBR (Part D) with a flow
141 rate of 0.6 L/min (0.02 m/s superficial gas velocity). Subsequently, N₂ was pumped
142 into the reactor to carry away the redundant TMA at the second step. After that,
143 synthetic air was pumped into the reactor to oxidize TMA and form the Al₂O₃ coating.
144 Finally, the extra oxygen was blown away by N₂ and then a new cycle can be started.
145 Duration of each step has been optimized as 3, 10, 3 and 10 minutes, respectively.
146



147

148 Fig. 1 Schematic illustration of the ALD set-up and process: (A) nitrogen gas tank; (B) and (C)
149 reactant tanks; (D) Fluidized Bed Reactor (FBR); (E) vibro-motors; (F) gas washers.

150 Effluent gases from the reactor were led through a double set of gas washers
151 (Part F) filled with mineral oil. The gas streams containing TMA was led through
152 separate gas washers to prevent reaction in the washers. Any TMA absorbed in the gas
153 washers was neutralized after the experiment. The effluent from the gas washers was
154 filtered using Pall Kleenpak pharmaceutical grade sterilizing filters to capture
155 elutriated nanoparticles. The pressure at the outlet was atmospheric, meaning that the
156 pressure in the column is slightly above atmospheric pressure. This is uncommon, as

157 most ALD is carried out at vacuum. More details about the reactor can be found in our
158 previous work¹⁴.

159

160 **2.3 Characterization**

161 The crystalline phases and compositions of the prepared samples were examined
162 by X-ray diffractometry (XRD) using a Bruker D4 Endeavor apparatus with a
163 graphite- monochromatized Cu Ka radiation at 40 kV and 40 mA. The 2θ ranges of all
164 the data sets are from 10 to 80° using step scan with a step size of 0.02° in 2θ and a
165 counting time of 1s per step. The micro-morphology and elemental mapping of the
166 samples were observed by using a JEOL/EO6500F Scanning Electron Microscope
167 (SEM) combined with Energy Dispersive X-ray spectroscopy (EDX), the voltage of
168 the EDX is 10KV and the spot size is 69 μm . Cross section SEM combined with EDX
169 was carried out on a FEI Nova Nano SEM for the Al_2O_3 coated samples, besides the
170 normal electric-beam for SEM, the equipment has an extra ion-beam for cut and mill
171 the target samples. Moreover, Transmission Electron Microscopy (TEM) analysis was
172 performed with an HRTEM JEOL 2010 high-resolution transmission electron
173 microscope in combination with EDX spectroscopy and a GATAN digital micrograph
174 with a slow-scan CCD camera.

175

176 **2.4 Optical properties**

177 A Perkin Elmer LS 50B spectrophotometer equipped with a Xe flash lamp as the
178 excitation source was used to conduct diffuse reflectance and photoluminescence (PL)
179 measurements. The reflection spectra were calibrated with the reflection of black felt
180 (reflection 3%) and white barium sulfate (BaSO_4 , reflection ~100%) in the
181 wavelength region of 230-700 nm. The excitation and emission slits were set at 15 nm.
182 All measurements were performed at room temperature.

183 The temperature dependent luminescence properties were measured by
184 home-built equipment. The emission spectra were measured in air with the
185 temperature increased from 300K to 600K. The emission spectrum was recorded from
186 480 nm to 700 nm with an excitation wavelength of 460 nm came from a Xe flash
187 lamp. The sample chamber was heated up with a rate of 10 K/min. The equipment
188 was maintained for extra 5 min before each measurement to hold a constant
189 temperature. The excitation and emission slits were set at 5 nm. Excitation spectra
190 were automatically corrected for the variation in the lamp intensity by a second
191 photomultiplier and a beam-splitter. All the spectra were measured with a scan speed
192 of 100 nm/min.

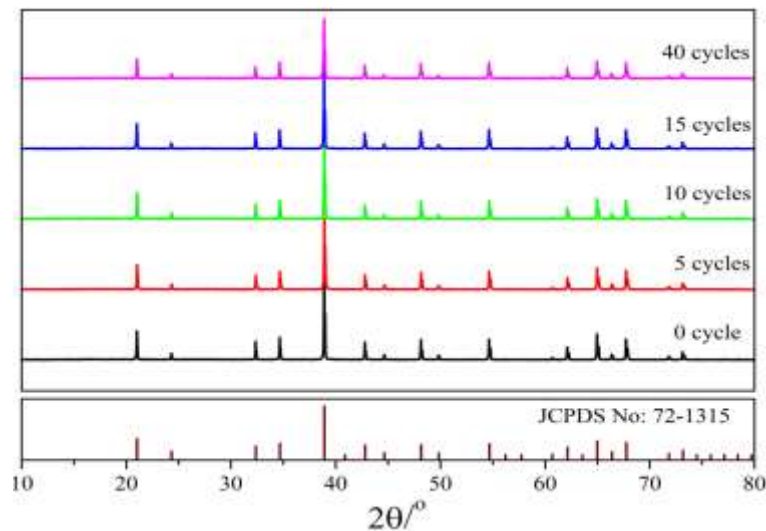
193

194 **3 Results and discussion**

195 **3.1 Phase composition**

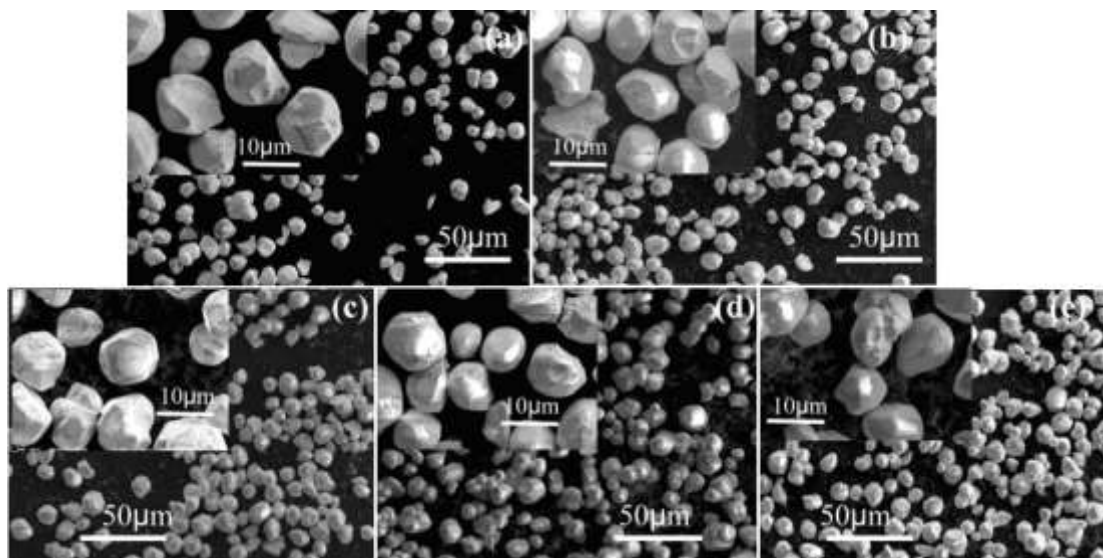
196 To study the impact of the ALD process on the phase composition of the selected
197 phosphor material, uncoated and Al_2O_3 coated Ce-doped YAG phosphor powders
198 were examined by XRD. As shown in Fig. 2, the diffraction peaks of all obtained
199 materials with or without coating are corresponding to $\text{Y}_3\text{Al}_5\text{O}_{12}$ with the garnet
200 structure (YAG) [Joint Committee on Powder Diffraction Standards (JCPDS) card No.

201 72-1315]. No obvious peak shifts or other impurity phases were detected after the
202 coating process, indicating that the sustainable ALD process has no obvious influence
203 on the phase and structure of the YAG:Ce phosphor. In addition, no diffraction peaks
204 characteristic for crystalline Al₂O₃ were detected, suggesting that the Al₂O₃ thin layer
205 should be amorphous phase since the crystalline phase of Al₂O₃ is expected only
206 above 900°C³⁰.
207



208
209 Fig.2 XRD patterns of the uncoated (0 cycle) and coated YAG:Ce phosphor powders after
210 different ALD cycles
211

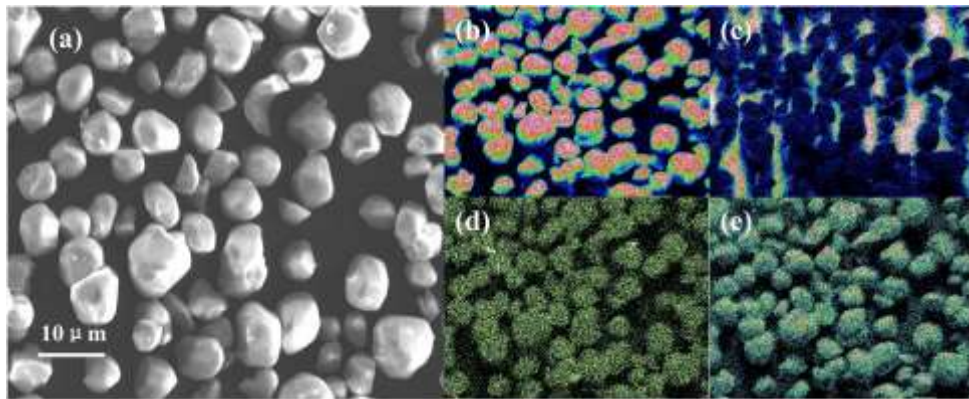
212 3.2 Particle morphology



213
214 Fig.3 SEM images of (a) the uncoated (0 cycle) and coated samples at different cycles (b) 5 cycles;
215 (c) 10 cycles; (d) 15 cycles; (e) 40 cycles under low and high magnification (insets)
216

217 SEM analysis was also carried out to investigate the influence of the ALD
218 process and alumina coating on the morphology of YAG:Ce particles. SEM
219 micrographs of the starting YAG:Ce sample [Fig. 3(a)] and Al₂O₃ coated YAG:Ce

220 particles at various cycles [Fig. 3(b)-3(e)] are shown in Fig. 3. The obtained samples
 221 with or without coating show similar micromorphology, all of which consist of
 222 uniform and spherical-like particles with a size range of 6-15 μm ($D_{50} = 11 \mu\text{m}$). There
 223 is no obvious difference between the coated and uncoated samples, implying that the
 224 Al_2O_3 ALD coating process has no influence on the morphology of the YAG:Ce
 225 particles, which should attribute to the ultrathin layer of the Al_2O_3 coating that can not
 226 be observed by normal SEM.
 227



228
 229 Fig. 4 SEM images of (a) YAG:Ce particle and corresponding elemental mapping of (b) Al, (c) Y,
 230 (d) Ce and (e) O.
 231

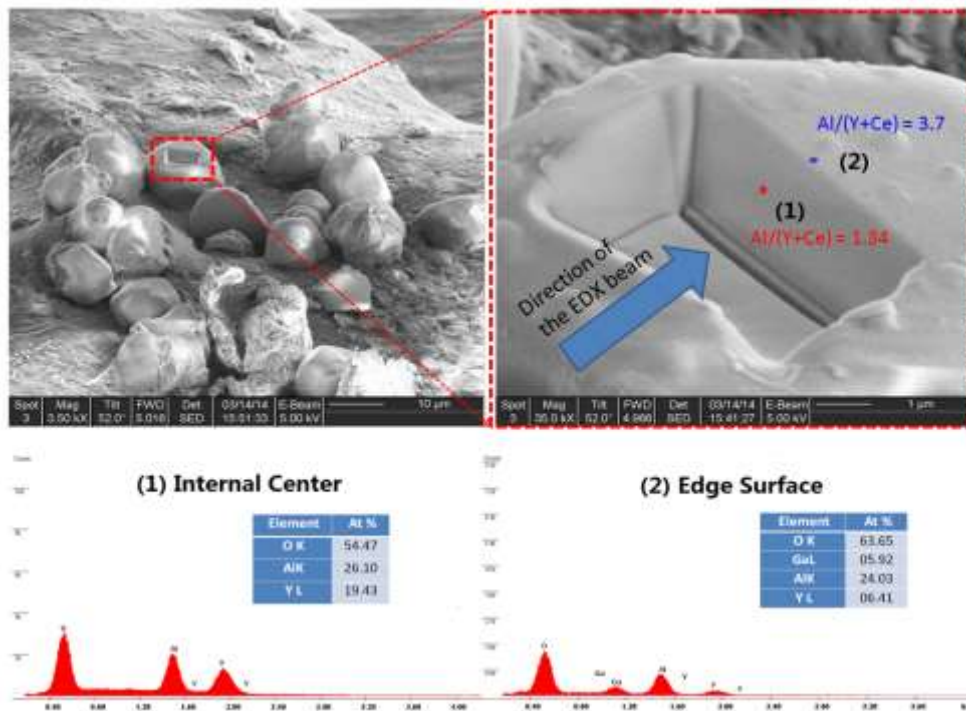
232 The elemental distribution of the coated YAG:Ce phosphor was mapped, as
 233 illustrated in Fig. 4. Results indicate that the Y, Al, O and Ce elements are uniformly
 234 distributed on the same particle, which confirms the uniform and homogeneous
 235 coating of alumina via ALD process in fluidized bed. Meanwhile, EDX analysis with
 236 SEM shows that the ratio of Al content divided by (Y + Ce) content grows from 1.38
 237 to 1.76 along with the increase of number of ALD cycles, as shown in Table. 1, which
 238 should be attributed to the increase of thickness of deposited Al_2O_3 layers with adding
 239 more ALD cycles. It needs to be mentioned that the ratio of $\text{Al}/(\text{Y}+\text{Ce})$ measured by
 240 EDX was relatively low compare to the ideal ratio (1.67) calculated for stoichiometric
 241 $\text{Y}_3\text{Al}_5\text{O}_{12}:\text{Ce}^{3+}$. However, impurities and defects are generally formed during the
 242 synthesis of $\text{Y}_3\text{Al}_5\text{O}_{12}$, and they exist within the crystals especially after doping with
 243 other cations^{31,32}.
 244

245 Table 1. The dependence of the $\text{Al}/(\text{Y}+\text{Ce})$ ratio on the number of ALD cycles, as obtained by
 246 EDX.

Cycle(s)	0	5	10	15	40
$\text{Al}/(\text{Y}+\text{Ce})$	1.38	1.43	1.51	1.60	1.76

247
 248 Furthermore, cross section SEM by dual beam was performed on the 40 cycles
 249 coated sample, as shown in Fig. 5. The signal of Gacomes from the ions beam, which
 250 was utilized to section the YAG:Ce particle. According to the EDX examination, the
 251 ratio of $\text{Al}/(\text{Y}+\text{Ce})$ at the surface (spot 2) turns out to be about 3.7, while that in the

252 bulk (spot 1) is about 1.34, which is in accordance with the Al/(Y+Ce) ratio
 253 determined for the uncoated sample (Table. 1). A higher level of Al/(Y+Ce) ratio at
 254 the surface than in the inner part of the particle, demonstrates that Al₂O₃ had been
 255 deposited on the surface of the phosphor particle and Al₂O₃ thin layer coating with
 256 ALD is highly feasible.
 257



258
 259 Fig.5 SEM cross section combined with EDX analysis of 40 cycles ALD coated YAG:Ce particle
 260

261 To further study the thickness of the ALD coating, TEM images of the coated
 262 samples were made. Unfortunately, the alumina layers covering the surface of the
 263 YAG:Ce particles were too thin to be observed for 5 and 10 cycles coated samples.
 264 But after 15 cycles of ALD coating, a 2 nm coating layer was detected and a clearer
 265 layer with 5 nm thickness was found for the sample coated with Al₂O₃ for 40 cycles
 266 by ALD process, TEM images are shown in Fig. 6. Besides, the alumina coating
 267 layers of both samples processed after 15 and 40 cycles were uniform, tight, and
 268 homogeneous, indicating that the ALD process performed in a fluidized bed is a
 269 promising approach for covering protective materials on phosphor particles.
 270 The thickness of the coating layer on the particles after 15 and 40 cycles is about 2 nm
 271 and 5 nm, respectively, from which the thickness of a single layer coating within one
 272 cycle can be estimated to be about 0.13 nm.

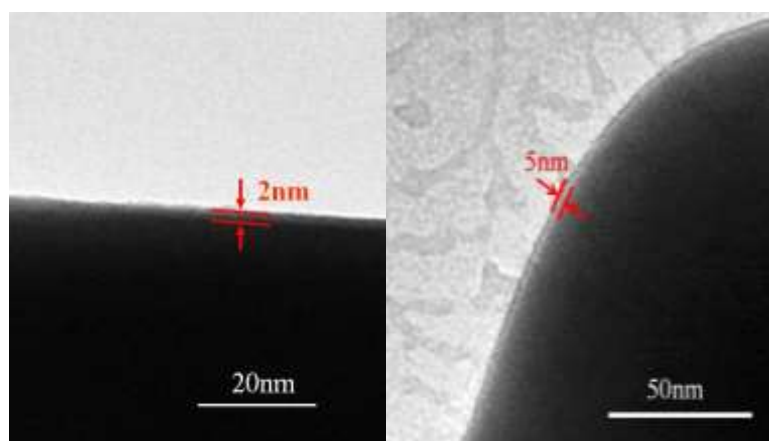


Fig. 6 TEM images of YAG:Ce particle coated with Al₂O₃ by ALD: (a) 15 cycles and (b) 40 cycles.

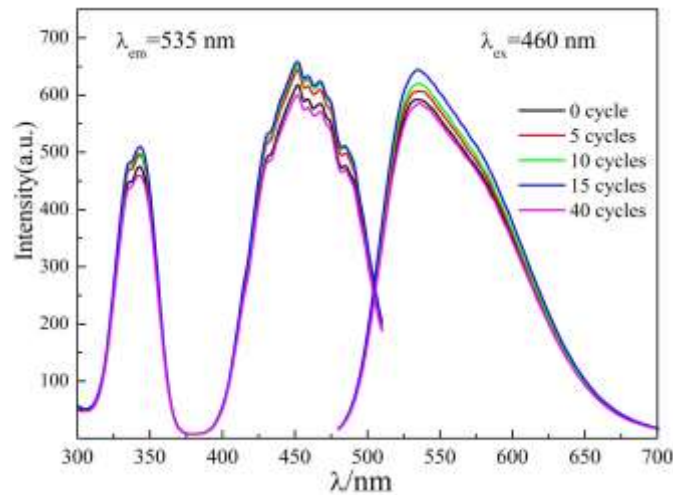
3.3 Luminescence properties

It has been confirmed that Al₂O₃ is an appropriate material for thermal protection via ALD process³³; however, it can also become an impeder for transfer of light, electrons, heat, humidity and so on³⁴. Thus, the luminescence properties of coated and uncoated YAG:Ce phosphor powders were carefully investigated in order to optimize the ALD cycle numbers and alumina coating thickness. Fig. 7 displays the luminescence spectra of uncoated YAG:Ce powder and Al₂O₃ coated YAG:Ce powders with different ALD cycle numbers. It can be seen that all samples, with or without coating, exhibit similar profiles of both excitation and emission bands with the same peak positions located at about 535 nm, indicating that the basic optical behavior of the phosphor has not been changed by the coating layer of alumina. The excitation spectra of all samples obtained upon monitoring 535 nm emission express two bands centered at around 450 nm and 350 nm respectively, which are corresponding to the transitions between the Ce³⁺ ground state (²F_{5/2}) and the 5d levels splitted by the crystal field with D₂ symmetry, which is in agreement with the report in the literature³⁵. Upon 460 nm excitation, all the samples show a broad band emission with the maximum peaks located at about 535 nm, which is assigned to the transition of the lowest 5d state to the 4f ground state (²F_{5/2}) of Ce³⁺ ions.

Some experimental results from Zhang et al.³⁶ confirm that the optical absorption behavior of phosphor composite materials can be largely dependent on the amount of Al₂O₃ compound. However, results achieved above indicate that the Al₂O₃ coating has no obvious affection on the luminescence properties of the sample. The reason might be that the alumina-coating layer is too thin to affect the light diffusion.

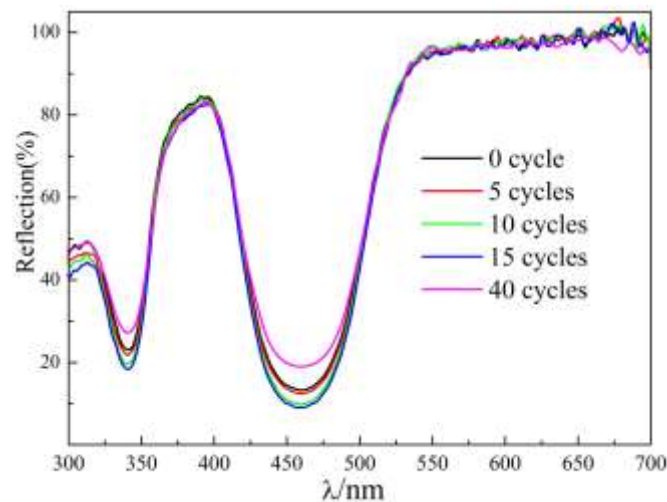
Nevertheless, the intensity of both excitation and emission bands show significant difference when comparing the uncoated and coated samples. The excitation and emission intensity continuously increase with increasing ALD cycle numbers, except for 40 cycles. After 40 cycles coating, the intensity dropped quite strongly and a value even lower than the uncoated phosphor was obtained. It can be concluded that alumina coating layer with controlled thickness of about 2 nm deposited via ALD process can benefit the luminescence properties, but too thick a coating will lower the excitation absorption as well as the emission radiation. The

307 enhancement of emission intensity can be attributed to an increased absorption
308 radiation, a larger quantum efficiency of absorbed radiation converted into emitted
309 radiation and an improved light outcoupling of emitted radiation. But when the
310 thickness of the covering went to 5 nm, the incident illumination and the emitted light
311 were largely obstructed by the over protective covering, thus the intensity of both
312 excitation and emission decreased rapidly.
313



314
315
316
317

Fig.7 Excitation and emission spectra of the uncoated and ALD coated YAG:Ce phosphor powder
(a) 0 cycle; (b) 5 cycles; (c) 10 cycles; (d) 15 cycles ; (e) 40 cycles.



318
319
320
321

Fig.8 Diffuse reflectance spectra of the uncoated (0 cycles) and Al₂O₃ coated YAG:Ce samples for
different ALD cycles (5-40 cycles)

322 A further illustration about the increased absorption strength is provided by the
323 diffuse reflectance spectra of coated and uncoated samples as shown in Fig. 8. In
324 comparison with the uncoated YAG:Ce samples, the Al₂O₃ coated ones with different
325 number of cycles exhibit similar absorption profiles and band widths, confirming that
326 the Al₂O₃ coating material has no significant effect on the absorption characteristics of

327 YAG:Ce phosphor powder. As compared to the uncoated phosphor, the reflection
 328 (around 340 and 455 nm) decreased (i.e. adsorption around 340 and 455 nm increased)
 329 for higher number of ALD cycles, except for the 40 cycles sample (Table 2). All of the
 330 above results are in agreement with the conclusion made from Fig. 7, further
 331 confirming that the covering thickness of the alumina coating should be optimized
 332 since a high amount of Al₂O₃ can hamper the light absorption as well as the light
 333 emission (Table 2).

334 The relative quantum efficiency is estimated by comparing the emission intensity
 335 (EI) of the coated sample with that of the uncoated YAG:Ce phosphor powder from
 336 the equation below:
 337

$$QE(\text{coated}) = \left[\frac{EI(\text{coated})}{EI(\text{uncoated})} \right] * \left[\frac{A(\text{uncoated})}{A(\text{coated})} \right] * QE(\text{uncoated})$$

338

339 Here, “QE” refers to the relative quantum efficiency; “EI” refers to the integrated
 340 area under the emission spectrum, which was obtained from the emission spectra in
 341 Fig. 7; “A” refers to the absorption intensity at excitation wavelength of 460 nm,
 342 which was calculated from the diffuse reflection spectra (A=1 - diffuse reflection for
 343 semi-infinite thick samples). The QE of the uncoated phosphor was taken 1.00. The
 344 calculated relative QE for the uncoated and coated samples are listed in Table. 2. The
 345 emission intensity of the phosphors increased with the adding of cycle numbers, and
 346 so does the relative quantum efficiency, with an exception of the 40 cycles coating
 347 sample. The higher relative quantum efficiency is attributed to surface passivation
 348 (resulting in less non-radiative transitions at defects) and easier extraction of the
 349 emitted light. In summary, the results indicate that the coated YAG:Ce samples
 350 processed with 10-15 cycles have better conversion abilities than the uncoated
 351 material.

352

353 Table 2. The absorption of 460 nm (excitation radiation) and the relative quantum efficiency of
 354 Al₂O₃ coated versus uncoated YAG: Ce phosphor powders.

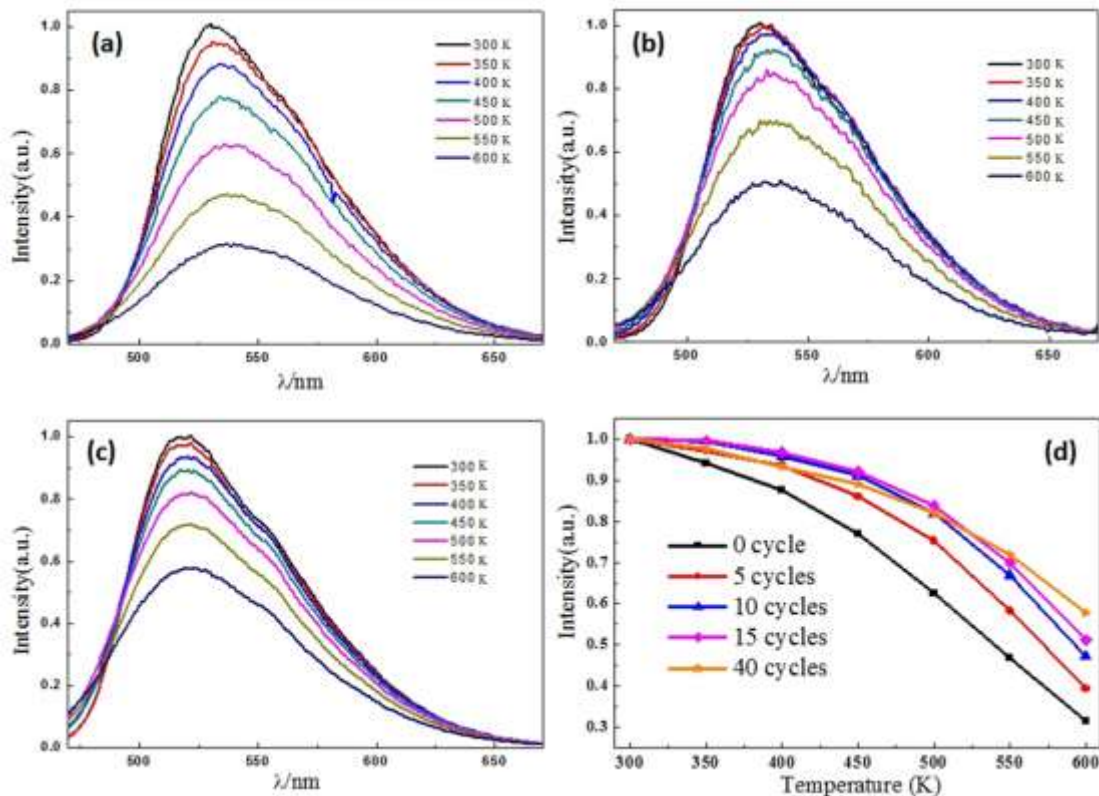
Number of coating cycles	Emission (arb. Units)	Absorption at 460 nm	Relative Quantum Efficiency
0 cycle	61639	0.93	1.00
5 cycles	63070	0.94	1.01
10 cycles	64222	0.94	1.03
15 cycles	66525	0.95	1.06
40 cycles	52938	0.93	0.96

355

356 3.4 Thermal stability

357 Fig. 9 displays the temperature-dependent emission spectra of the uncoated and
 358 coated YAG:Ce phosphor powders prepared by ALD method, combined with the
 359 summary of the dependence of the emission intensity in sample temperature (Fig.
 360 9(d)). When compared with the uncoated YAG:Ce phosphor, the peak emission

361 wavelength of all the coated samples shows a red shift for higher sample temperature,
 362 which can be explained by increased re-absorption due to more efficient energy
 363 transfer at high temperature. When excited by 460 nm radiation, the integrated
 364 emission intensities of all the samples continuously decreased with increasing sample
 365 temperature from 300K to 600K, showing a typical thermal quenching behavior,
 366 which is a normal phenomenon for all kinds of phosphors³. In comparison with the
 367 uncoated sample, a remarkable development in temperature-dependent characteristic
 368 of Ce³⁺ emission of coated phosphors can be observed, demonstrating that the thermal
 369 stability of YAG:Ce phosphor can be significantly improved by coating protective
 370 alumina layers via ALD method.
 371

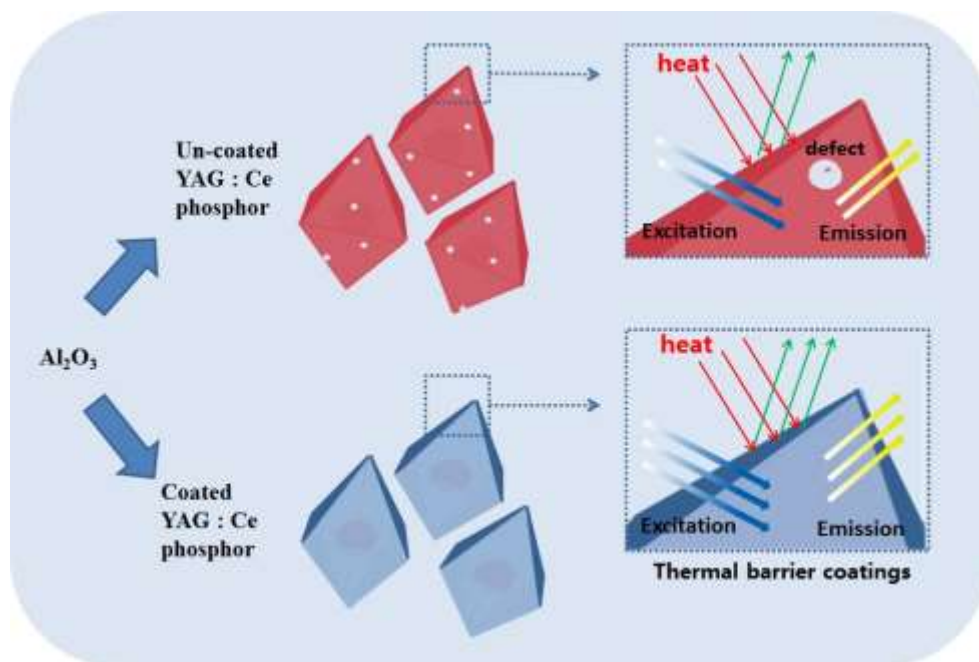


372
 373 Fig.9 Temperature-dependent PL spectra for samples with various coating cycles: (a) uncoated, (b)
 374 15 cycles, (c) 40 cycles, and (d) summarization of the PL intensity of all samples, under excitation
 375 wavelengths of 460 nm.
 376

377 Fig. 9(d) summarizes the emission intensity at different temperatures of all
 378 samples according to the temperature-dependent emission spectra. The intensity was
 379 normalized to that exhibited at room temperature for each sample. At the starting
 380 temperature of 300K, all five samples are normalized as the same emission intensity
 381 of about 100% for comparison. However, already after 50 degrees temperature
 382 increment, remarkable changes have been observed for the alumina coated YAG:Ce
 383 phosphor powders. More than 5% decrease was found for the uncoated phosphor,
 384 while the intensity of the 5 cycles sample dropped only about 2% and the intensity of
 385 samples with 10 and 15 cycles coating remained more or less constant. The thermal

386 stability of the coated phosphor has been remarkably improved even for only 5 ALD
387 coating cycles, and for higher ALD cycle numbers, better thermal stability can be
388 achieved. Especially at elevated temperature of 550K and 600K, the emission
389 intensity of the uncoated phosphor dropped rapidly to 47% and 32%, while that of the
390 40 cycles coated sample remained at a high value of 70% and 57%, respectively. The
391 enhancement of thermal stability should be attributed to the effect of the thermal
392 barrier coating of alumina formed by ALD process, which can keep the inner
393 phosphor particles from directly exposure to the hot environment and protect Ce^{3+}
394 against oxidization to Ce^{4+} .

395 A phenomenon needs to be mentioned is that a lower relative emission intensity
396 was exhibited by sample with 40 cycles coating than that of samples with 10 and 15
397 cycles coating during the temperature range of 300K to 500K, indicating that high
398 thickness alumina layer coatings might impede the luminescence properties of the
399 phosphor below 550 K. It has been reported that Al_2O_3 sometimes works like an
400 insulator that can barrier the transfer of light, electrons or heat³⁴. This conclusion is in
401 accordance with the results of the luminescence property analysis discussed above.
402



403
404 Fig.10 Schematic diagram of enhancing of luminescence intensity coating Al_2O_3 layer by ALD
405 process in YAG:Ce host.
406

407 Fig. 10 schematically illustrates the mechanism of the enhancing emission
408 intensity and thermal stability from the protective alumina layer for YAG:Ce phosphor.
409 Firstly, coating the YAG:Ce phosphor powders with a thin Al_2O_3 layer with an
410 appropriate thickness can increase the quantum efficiency due to reduced number of
411 surface defects, enhance the light absorption and form a thermal barrier coating.
412 Secondly, Al_2O_3 is kind of wide band gap oxide material, which could confine the
413 inside excitation of the phosphor and suppress the ion-ion energy transfer (short range
414 Forster transfer), ultimately decrease the non-radiative recombination. Finally, the

415 lack of Ce ion in the outer coating shell would effectively suppress the energy transfer
416 from the inner part of the particle to the outside surface. Combined the above three, the
417 quantum efficiency, emission intensity as well as thermal stability of the phosphor can
418 be remarkably improved.

419

420 **4 Conclusions**

421 The yellow-emitting YAG:Ce LED phosphor powders have been successfully
422 coated with a thin Al₂O₃ layer via the approach of fluidized bed reactor ALD. With
423 the controllable deposition in the fluidized bed ALD reactor, designable thickness of
424 the alumina-coating layer can be obtained. With the appropriate Al₂O₃ coating layer
425 thickness, an improvement of luminescence properties and thermal stability of the
426 phosphor can be achieved without any change in bulk behavior. The uniform and
427 stable Al₂O₃ coating can reduce the number of surface defects of the phosphor
428 particles and might enhance the quantum efficiency, consequently improving the
429 optical performance. The thermal stability was improved gradually with the increase
430 of the coating layer thickness, since the coated layer can act as a barrier to decrease
431 the thermal quenching, resulting in high thermal resistance of the YAG:Ce material.
432 For all the samples examined, the one with 15 cycles coating exhibited the best
433 characteristics, from which can be concluded that the amount of the alumina coating
434 needs to be precisely controlled.

435

436 **Acknowledgement**

437 The authors would like to thank the China Scholarship Council (No
438 201206370063), the Education Department of Hunan Province (No 14C0577), Hunan
439 Natural Science Foundation (2016JJ3065), and Hunan Agricultural University (No
440 13YJ02, No 14YJ05) for financial support.

441

442 **Reference:**

443

- 444 1. T. Jüstel, H. Nikol and C. Ronda, *Angewandte Chemie International Edition*, 1998, **37**,
445 3084-3103.
- 446 2. Y. Li, M. Gecevicius and J. Qiu, *Chemical Society Reviews*, 2016, **45**, 2090-2136.
- 447 3. G. Li, Y. Tian, Y. Zhao and J. Lin, *Chemical Society Reviews*, 2015, **44**, 8688-8713.
- 448 4. H. Kim, C. Yun, S. W. Jeon, J. K. Lee and J. P. Kim, *Optical Materials*, 2016, **53**, 48-53.
- 449 5. J. Zhang, Y. Fan, Z. Chen, S. Yan, J. Wang, P. Zhao, B. Hao and M. Gai, *Journal of Rare Earths*,
450 2015, **33**, 922-926.
- 451 6. J. P. Kim and S. B. Song, *Applied Surface Science*, 2011, **257**, 2159-2163.
- 452 7. H. Yang, X. Wang, G. Duan, Y. Cui, L. Shen, Y. Xie and H. Sangdo, *Materials Letters*, 2004, **58**,
453 2374-2376.
- 454 8. H. S. Park, G. Dodbiba, L. F. Cao and T. Fujita, *Journal of Physics: Condensed Matter*, 2008, **20**,
455 204105.
- 456 9. H. Zhu, H. Yang, W. Fu, P. Zhu, M. Li, Y. Li, Y. Sui, S. Liu and G. Zou, *Materials Letters*, 2008, **62**,
457 784-786.
- 458 10. K. L. Choy, *Progress in Materials Science*, 2003, **48**, 57-170.

- 459 11. J. Chao, L. Fei, L. Hua, H. Shao-liu, L. Bo and W. You-qing, *Applied Surface Science*, 2005, **246**,
460 207-213.
- 461 12. O. J. Kilbury, K. S. Barrett, X. Fu, J. Yin, D. S. Dinair, C. J. Gump, A. W. Weimer and D. M. King,
462 *Powder Technology*, 2012, **221**, 26-35.
- 463 13. N. Avci, J. Musschoot, P. F. Smet, K. Korthout, A. Avci, C. Detavernier and D. Poelman, *Journal*
464 *of The Electrochemical Society*, 2009, **156**, J333-J337.
- 465 14. R. Beetstra, U. Lafont, J. Nijenhuis, E. M. Kelder and J. R. van Ommen, *Chemical Vapor*
466 *Deposition*, 2009, **15**, 227-233.
- 467 15. M. Ritala, K. Kukli, A. Rahtu, P. I. Räisänen, M. Leskelä, T. Sajavaara and J. Keinonen, *Science*,
468 2000, **288**, 319-321.
- 469 16. Z. Wang, H. Guo, F. Shen, G. Yang, Y. Zhang, Y. Zeng, L. Wang, H. Xiao and S. Deng,
470 *Chemosphere*, 2015, **119**, 646-653.
- 471 17. J. Lee, D. H. K. Jackson, T. Li, R. E. Winans, J. A. Dumesic, T. F. Kuech and G. W. Huber, *Energy &*
472 *Environmental Science*, 2014, **7**, 1657-1660.
- 473 18. M. Zeng, X. Peng, J. Liao, G. Wang, Y. Li, J. Li, Y. Qin, J. Wilson, a. song and S. Lin, *Physical*
474 *Chemistry Chemical Physics*, 2016, DOI: 10.1039/C6CP01299J.
- 475 19. L. H. Kim, Y. J. Jeong, T. K. An, S. Park, J. H. Jang, S. Nam, J. Jang, S. H. Kim and C. E. Park,
476 *Physical Chemistry Chemical Physics*, 2016, **18**, 1042-1049.
- 477 20. X. Dong, X. Fang, M. Lv, B. Lin, S. Zhang, J. Ding and N. Yuan, *Journal of Materials Chemistry A*,
478 2015, **3**, 5360-5367.
- 479 21. J. D. Ferguson, A. W. Weimer and S. M. George, *Chemistry of Materials*, 2000, **12**, 3472-3480.
- 480 22. J. Lu, Y. H. Wang, J. B. Zang and Y. N. Li, *Applied Surface Science*, 2007, **253**, 3485-3488.
- 481 23. K. Nevalainen, R. Suihkonen, P. Eteläaho, J. Vuorinen, P. Järvelä, N. Isomäki, C. Hintze and M.
482 Leskelä, *Journal of Vacuum Science & Technology A*, 2009, **27**, 929-936.
- 483 24. P. A. Williams, C. P. Ireland, P. J. King, P. A. Chater, P. Boldrin, R. G. Palgrave, J. B. Claridge, J. R.
484 Darwent, P. R. Chalker and M. J. Rosseinsky, *Journal of Materials Chemistry*, 2012, **22**,
485 20203-20209.
- 486 25. D. M. King, J. Li, X. Liang, S. I. Johnson, M. M. Channel and A. W. Weimer, *Crystal Growth &*
487 *Design*, 2009, **9**, 2828-2834.
- 488 26. D. M. King, X. Liang, P. Li and A. W. Weimer, *Thin Solid Films*, 2008, **516**, 8517-8523.
- 489 27. J. Zhao and Y. Wang, *Nano Energy*, 2013, **2**, 882-889.
- 490 28. L. Xiong, Y. Xu, T. Tao, X. Du and J. Li, *Journal of Materials Chemistry*, 2011, **21**, 4937-4944.
- 491 29. D. Valdesueiro, M. K. Prabhu, C. Guerra-Nunez, C. S. S. Sandeep, S. Kinge, L. D. A. Siebbeles, L.
492 C. P. M. de Smet, G. M. H. Meesters, M. T. Kreutzer, A. J. Houtepen and J. R. van Ommen, *The*
493 *Journal of Physical Chemistry C*, 2016, **120**, 4266-4275.
- 494 30. H. J. Kim, M. W. Kim, H. s. Kim, H. S. Kim, S. H. Kim, S. W. Lee, B. H. Choi, B. K. Jeong and H. h.
495 Lee, *Molecular Crystals and Liquid Crystals*, 2006, **459**, 239/[519]-245/[525].
- 496 31. H. K. Yang, H. M. Noh and J. H. Jeong, *Solid State Sciences*, 2014, **27**, 43-46.
- 497 32. M. Kučera, K. Nitsch, M. Nikl and M. Hanuš, *Radiation Measurements*, 2010, **45**, 449-452.
- 498 33. V. Edlmayr, M. Moser, C. Walter and C. Mitterer, *Surface and Coatings Technology*, 2010, **204**,
499 1576-1581.
- 500 34. A. Kafizas and I. P. Parkin, *Chemical Society Reviews*, 2012, **41**, 738-781.
- 501 35. Z. Zhi, L. Suqin, W. Fengchao and L. Younian, *Journal of Physics D: Applied Physics*, 2012, **45**,
502 195105.

503 36. C. Zhang and J. Lin, *Chemical Society Reviews*, 2012, **41**, 7938-7961.